Monthly Notices of the ROYAL ASTRONOMICAL SOCIETY
MNRAS **451,** 3882–3897 (2015) doi:10.1093/mnras/stv1208

Multiband optical–NIR variability of blazars on diverse time-scales

Aditi Agarwal,[1,2]★ Alok C. Gupta,[1,2,3]★† R. Bachev,[4]★ A. Strigachev,[4] E. Semkov,[4] Paul J. Wiita,[5] M. Böttcher,[6] S. Boeva,[4] H. Gaur,[3,7] M. F. Gu,[3] S. Peneva,[4] S. Ibryamov[4] and U. S. Pandey[2]

[1]*Aryabhatta Research Institute of Observational Sciences (ARIES), Manora Peak, Nainital 263002, India*
[2]*Department of Physics, DDU Gorakhpur University, Gorakhpur 273009, India*
[3]*Key Laboratory for Research in Galaxies and Cosmology, Shanghai Astronomical Observatory, Chinese Academy of Sciences, 80 Nandan Road, Shanghai 200030, China*
[4]*Institute of Astronomy and National Astronomical Observatory, Bulgarian Academy of Sciences, 72 Tsarigradsko Shosse Blvd, 1784 Sofia, Bulgaria*
[5]*Department of Physics, The College of New Jersey, P.O. Box 7718, Ewing, NJ 08628, USA*
[6]*Centre for Space Research, North-West University, Potchefstroom 2520, South Africa*
[7]*Inter-University Centre for Astronomy and Astrophysics (IUCAA), Ganeshkhind, Pune 411 007, India*

Accepted 2015 May 21. Received 2015 April 29; in original form 2014 November 12

ABSTRACT

To search for optical variability on a wide range of time-scales, we have carried out photometric monitoring of two flat spectrum radio quasars, 3C 454.3 and 3C 279, plus one BL Lac, S5 0716+714, all of which have been exhibiting remarkably high activity and pronounced variability at all wavelengths. CCD magnitudes in *B*, *V*, *R*, and *I* passbands were determined for ∼7000 new optical observations from 114 nights made during 2011–2014, with an average length of ∼4 h each, at seven optical telescopes: four in Bulgaria, one in Greece, and two in India. We measured multiband optical flux and colour variations on diverse time-scales. Discrete correlation functions were computed among *B*, *V*, *R*, and *I* observations, to search for any time delays. We found weak correlations in some cases with no significant time lags. The structure function method was used to estimate any characteristic time-scales of variability. We also investigated the spectral energy distribution of the three blazars using *B*, *V*, *R*, *I*, *J*, and *K* passband data. We found that the sources almost always follow a bluer-when-brighter trend. We discuss possible physical causes of the observed spectral variability.

Key words: galaxies: active – BL Lacertae objects: general – BL Lacerate objects: individual: 3C 454.3 – BL Lacerate objects: individual: 3C 279 – BL Lacerate objects: individual: S5 0716+714.

1 INTRODUCTION

Some of the brightest radio-loud Active Galactic Nuclei (AGN), called blazars, are understood to have relativistic jets viewed at an angle of $\leq 10^{\circ}$ from the line of sight (LOS; e.g. Urry & Padovani 1995), which amplifies chaotic flux variability spanning the entire electromagnetic (EM) spectrum. The blazar class includes BL Lacertae objects (BL Lacs) and flat spectrum radio quasars (FSRQs). BL Lacs exhibit non-thermal continuum emission with essentially featureless optical spectra, whereas FSRQs have the prominent emission lines characteristic of quasars. These sub-classes differ in wavelength-dependent optical polarization properties, with BL Lacs displaying increased polarization towards blue which could be due to some intrinsic phenomenon related to the jet-emitting region, while the FSRQs show an opposite trend, likely arising from the contribution of unpolarized thermal radiation from the accretion disc and the surrounding regions at shorter wavelengths (Smith 1996; Raiteri et al. 2012). The observational properties of the blazar class of AGN include broad-band continuum spectral energy distributions (SEDs) dominated by non-thermal emission from radio through γ-rays, a relativistic jet, extreme luminosity due to Doppler boosting of the relativistic jet emissions, a high degree of polarization, superluminal motion of some of their radio components (e.g. Aller, Aller & Hughes 1992; Aller, Aller & Hughes 2003; Andruchow, Cellone & Romero 2005), and flux variability on time-scales of hours to years at all wavelengths.

The pronounced variability throughout the EM spectrum (from radio to GeV or even TeV energies) at all accessible time-scales ranging from few minutes through months to decades, has been generally divided into three classes: flux changes observed from few tens of minutes to less than a day are commonly called

★E-mail: aditi@aries.res.in (AA); acgupta30@gmail.com (ACG); blazonstone@gmail.com (RB)
† CAS Visiting Fellow.

Table 1. Details of telescopes and instruments.

Site:	A	B	C	D/G	E	F
Scale:	0.2825 arcsec pixel^{-1}	0.258 arcsec pixel^{-1}	1.079 arcsec pixel^{-1}	0.330 arcsec pixel^{-1}[a]	0.535 arcsec pixel^{-1}	0.37 arcsec pixel^{-1}
Field:	9.6 arcmin × 9.6 arcmin	5.76 arcmin × 5.59 arcmin	73.66 arcmin × 73.66 arcmin	16.8 arcmin × 16.8 arcmin	18 arcmin × 18 arcmin	13 arcmin × 13 arcmin
Gain:	2.687 e$^-$/ADU	1.0 e$^-$/ADU	1.0 e$^-$/ADU	1.0 e$^-$/ADU	1.4 e$^-$/ADU	10 e$^-$/ADU
Read out noise:	8.14 e$^-$ rms	2.0 e$^-$ rms	9.0 e$^-$ rms	8.5 e$^-$ rms	4.1 e$^-$ rms	5.3 e$^-$ rms
Typical seeing :	1–2 arcsec	1.5–3.5 arcsec	2–4 arcsec	1.5–3.5 arcsec	1.2–2.0 arcsec	1–2.8 arcsec

Notes. A: 1.3-m Ritchey–Chretien telescope at Skinakas Observatory, University of Crete, Greece.
B: 2-m Ritchey–Chretien telescope at National Astronomical Observatory, Rozhen, Bulgaria.
C: 50/70-cm Schmidt telescope at National Astronomical Observatory, Rozhen, Bulgaria.
D: 60-cm Cassegrain telescope at Astronomical Observatory Belogradchik, Bulgaria.
E: 1.30-m Ritchey–Chretien Cassegrain optical telescope, ARIES, Nainital, India.
F: 1.04-m Sampuranand Telescope, ARIES, Nainital, India.
G: 60-cm Cassegrain telescope at National Astronomical Observatory, Rozhen, Bulgaria.
[a]With a binning factor of 1 × 1.

Table 2. Results of IDV observations of the blazars. The full version of this table is available in the online version of this paper in the Supporting Information section.

Source	Date	Band	N	$\sigma_{(BL-S_A)}$	$\sigma_{(BL-S_B)}$	$\sigma_{(S_A-S_B)}$	F-test $F_1, F_2, F, F_c(0.99), F_c(0.999)$	Variable	C	A per cent
3C 454.3	29-10-2013	B	23	0.0772	0.0784	0.0310	6.2, 6.4, 6.28, 2.79, 3.98	V	2.5065	26.98
		V	24	0.0200	0.0347	0.0278	0.5, 1.6, 1.04, 2.72, 3.85	NV	0.9840	–
		R	24	0.1035	0.0222	0.1080	0.9, 0.04, 0.47, 2.72, 3.85	NV	0.5819	–
		I	24	0.0207	0.0249	0.0179	1.3, 1.9, 1.63, 2.72, 3.85	NV	1.2723	–
		$(B-V)$	23	0.0701	0.0627	0.0353	3.9, 3.1, 3.55, 2.79, 3.98	V	1.8807	23.62
		$(B-I)$	23	0.0750	0.0674	0.0321	5.5, 4.4, 4.93, 2.79, 3.98	V	2.2177	23.25
		$(V-R)$	24	0.1072	0.0334	0.1050	1.0, 0.1, 0.57, 2.72, 3.85	NV	0.6695	–
		$(R-I)$	24	0.1098	0.0306	0.1136	0.9, 0.1, 0.50, 2.72, 3.85	NV	0.6176	–

Notes. V: variable, NV: non-variable.

intraday variability (IDV; Kinman 1975; Wagner & Witzel 1995; Clements, Jenks & Torres 2003; Rector & Perlman 2003; Xie et al. 2004; Gupta et al. 2008a) or intranight variability or microvariability; those from several days to few weeks are known as short-term variability (STV; Kranich et al. 1999; Lainela et al. 1999), while long-term variability (LTV) covers flux changes from several months to many years (e.g. Jurkevich 1971; Terrell & Olsen 1972; Sillanpää et al. 1988; Liu, Xie & Bai 1995; Fan & Lin 2000; Gupta et al. 2004).

Blazar SEDs exhibit double-peaked structures (Fossati et al. 1998). The low-frequency component is typically observed to peak in the near-infrared (NIR) or optical bands for low-synchrotron-peaked blazars [LSPs, consisting of FSRQs and low-frequency-peaked BL Lac objects (LBLs)] and in the UV or X-rays for high-synchrotron-peaked blazars (HSPs, generally belonging to the class of high-frequency-peaked BL Lac objects, HBLs; Giommi, Ansari & Micol 1995). Blazars whose SED peaks are located at intermediate frequencies sometimes are termed intermediate-synchrotron-peaked blazars (ISPs; Sambruna, Maraschi & Urry 1996). Specifically, Abdo et al. (2010) defined non-thermal-dominated AGN based on the peak frequency of their synchrotron hump, ν_{peak}, such that LSP sources are those with $\nu_{peak} \leq 10^{14}$ Hz, ISPs have $10^{14} < \nu_{peak} < 10^{15}$ Hz, and HSPs have $\nu_{peak} \geq 10^{15}$ Hz. The second SED component extends up to the γ-ray bands, peaking at GeV energies for LBLs and FSRQs, and at TeV energies for HBLs. The low-energy component is commonly ascribed to synchrotron radiation from ultrarelativistic electrons in the relativistic jet. The high-energy component is often interpreted as due to Compton upscattering of low-energy photons by the same electrons in the jet (leptonic models; Padovani & Giommi 1995), although hadronic models, in which protons are assumed to be accelerated to ultrarelativistic energies and γ-ray emission results from proton synchrotron radiation and photo–pion production induced processes, remain viable (e.g. Böttcher et al. 2013).

The key motivation of this work was to search for optical flux and colour variability of 3C 454.3, S5 0716+714, and 3C 279 on diverse time-scales, including analyses of colour–magnitude variations, interband cross-correlations, and optical/NIR SEDs. Here we report optical observations of the targets in the B, V, R, and I optical bands monitored from 2011 to 2014.

2 OBSERVATIONS AND DATA REDUCTIONS

Our optical photometric observations of the blazars were performed in the B, V, R, and I passbands, using seven telescopes, two in India, one in Greece, and four in Bulgaria, all equipped with CCD detectors. The details of the telescopes, instruments, and other parameters used are given in Table 1. Complete details of the observations are listed in Tables 1–3 of supplementary material available for this article. IDV light curves (LCs), covering nights when the observation runs were at least ∼4 h in the B, V, R, and I passbands, are displayed in Figs 1–3. Photometric observations obtained with telescopes listed in Table 1, were bias subtracted and twilight flat fielded followed by cosmic ray removal using standard packages (MIDAS,[1] IRAF[2]). Aperture photometry was performed using standard IRAF and Dominion Astronomical Observatory Photometry (DAOPHOT II)

[1] ESO-MIDAS is the acronym for the European Southern Observatory Munich Image Data Analysis System which is developed and maintained by European Southern Observatory.
[2] IRAF is distributed by the National Optical Astronomy Observatories, which are operated by the Association of Universities for Research in Astronomy, Inc., under cooperative agreement with the National Science Foundation.

Table 3. Results for IDV studies displaying magnitude changes in each band.

Source	Band	Faintest mag	Date (Max)	Brightest mag	Date (Min)	Δm
3C 4543.3	*B*	16.78	04-11-2013	14.45	25-09-2013	2.33
	V	15.84	04-11-2013	13.86	25-09-2013	1.98
	R	15.40	04-01-2014	13.14	24-06-2014	2.26
	I	15.00	04-01-2014	12.74	25-09-2013	2.26
3C 279	*R*	14.56	10-04-2014	14.45	03-02-2014	0.11
S5 0716+714	*B*	14.07	14-12-2012	13.19	23-03-2012	0.88
	V	14.75	21-01-2012	12.63	20-03-2012	2.12
	R	14.82	04-01-2014	12.25	20-03-2012	2.69
	I	13.74	21-01-2012	11.74	20-03-2012	2.00

Notes. Column 1 is the source name, column 2 indicates the band in which observations were taken, column 3 represents the maximum magnitude attained by the source in the filter mentioned in previous column on a particular date which is given in column 4, followed by minimum magnitude value and respective date in column 5 and column 6 and finally the net magnitude change during IDV observations is given in column 7.

software (Stetson 1987, 1992) routines. The calibrated LCs are displayed in Figs 1–3. Data from the Steward Observatory (SO) spectropolarimetric monitoring project[3] led by P. Smith were also used in the optical *V* band. The SMARTS[4] photometric data and LCs for all the blazars are publicly available on the web (Bailyn et al. 1999).We have taken data from the SMARTS web archive for each of the blazars in the *B*, *V*, *R*, and *I* passbands for a few nights for the purpose of investigating STV. We also used archived data from the *J* and *K* bands for studying variations in the optical/NIR SED.

3 ANALYSIS TECHNIQUES

3.1 Variability detection criterion

The IDV of blazars was examined employing both the popularly used *C*-statistic and the more reliable *F*-test.

3.1.1 C-test

The *C*-statistic was introduced by Romero, Cellone & Combi (1999), using the variability detection parameter, *C*, defined as the average of C_1 and C_2 with

$$C_1 = \frac{\sigma(\mathrm{BL} - S_\mathrm{A})}{\sigma(S_\mathrm{A} - S_\mathrm{B})}, C_2 = \frac{\sigma(\mathrm{BL} - S_\mathrm{B})}{\sigma(S_\mathrm{A} - S_\mathrm{B})}. \quad (1)$$

Here (BL−S_A), (BL−S_B), and (S_A−S_B) are the differential instrumental magnitudes of the blazar and standard star A (S_A), the blazar and standard star B (S_B), and S_A versus S_B determined using aperture photometry of the source and comparison stars, whereas σ(BL−S_A), σ(BL−S_B), and σ(S_A−S_B) are observational scatters of the differential instrumental magnitudes of the blazar−S_A, blazar−S_B, and S_A−S_B, respectively. We observed three or more comparison stars of which we selected those two standard stars for which σ(S_A−S_B) was minimal. A value of $C \geq 2.57$ implies that the source is variable at a nominal confidence level of >99 per cent.

3.1.2 F-test

As pointed out by de Diego (2010) the *C*-test is not a true statistic and is usually too conservative in quantifying variability. The *F*-test is a more powerful and properly distributed statistic that can be used to check the presence of microvariability or IDV. The *F* values compare two sample variances and are calculated as

$$F_1 = \frac{\mathrm{Var}(\mathrm{BL} - S_\mathrm{A})}{\mathrm{Var}(S_\mathrm{A} - S_\mathrm{B})},$$

$$F_2 = \frac{\mathrm{Var}(\mathrm{BL} - S_\mathrm{B})}{\mathrm{Var}(S_\mathrm{A} - S_\mathrm{B})}.$$

Here (BL−S_A), (BL−S_B), and (S_A−S_B) are the differential instrumental magnitudes of blazar and standard A, blazar and standard B, and standard A and standard B, respectively, while Var(BL−S_A), Var(BL−S_B), and Var(S_A−S_B) are the variances of differential instrumental magnitudes.

The *F* value is compared with a critical value, $F^{(\alpha)}_{\nu_\mathrm{bl},\nu_*}$, where ν_bl and ν_*, respectively, denote the number of degrees of freedom calculated as the number of measurements, *N*, minus 1 ($\nu = N - 1$), while α corresponds to the significance level, which we have set as 0.1 and 1 per cent (i.e 3σ and 2.6σ) in our analysis. We take the average of F_1 and F_2 to find a mean observational *F* value and compare it with the critical *F* value. If the mean *F* value is larger than the critical value, the null hypothesis (i.e. that of no variability) is discarded. The modest number of measurements we could make in most bands on most nights made the use of the ANOVA technique (de Diego 2010) in-feasible. In order to claim the presence or absence of variability during the observations, we have used the *F*-test at 0.99 confidence level.

3.1.3 Percentage amplitude variation

The percentage variation on a given night is calculated by using the variability amplitude parameter *A*, introduced by Heidt & Wagner (1996), and defined as

$$A = 100 \times \sqrt{(A_\mathrm{max} - A_\mathrm{min})^2 - 2\sigma^2}(\text{per cent}), \quad (2)$$

where A_max and A_min are the maximum and minimum values in the calibrated LCs of the blazar, and σ is the average measurement error. The calculated *C*- and *F*-statistics and the variability amplitude parameters, *A*, are presented in Table 2 whose full version is available in the supplementary material to this article. Nightly LCs and colour indices are listed as variable if $F > F_\mathrm{c}(0.99)$, though rarely do they satisfy the $F > F_\mathrm{c}(0.999)$ or the $C > 2.57$ criteria.

[3] http://james.as.arizona.edu/~psmith/Fermi/
[4] http://www.astro.yale.edu/smarts/glast/3C454.3lc.html

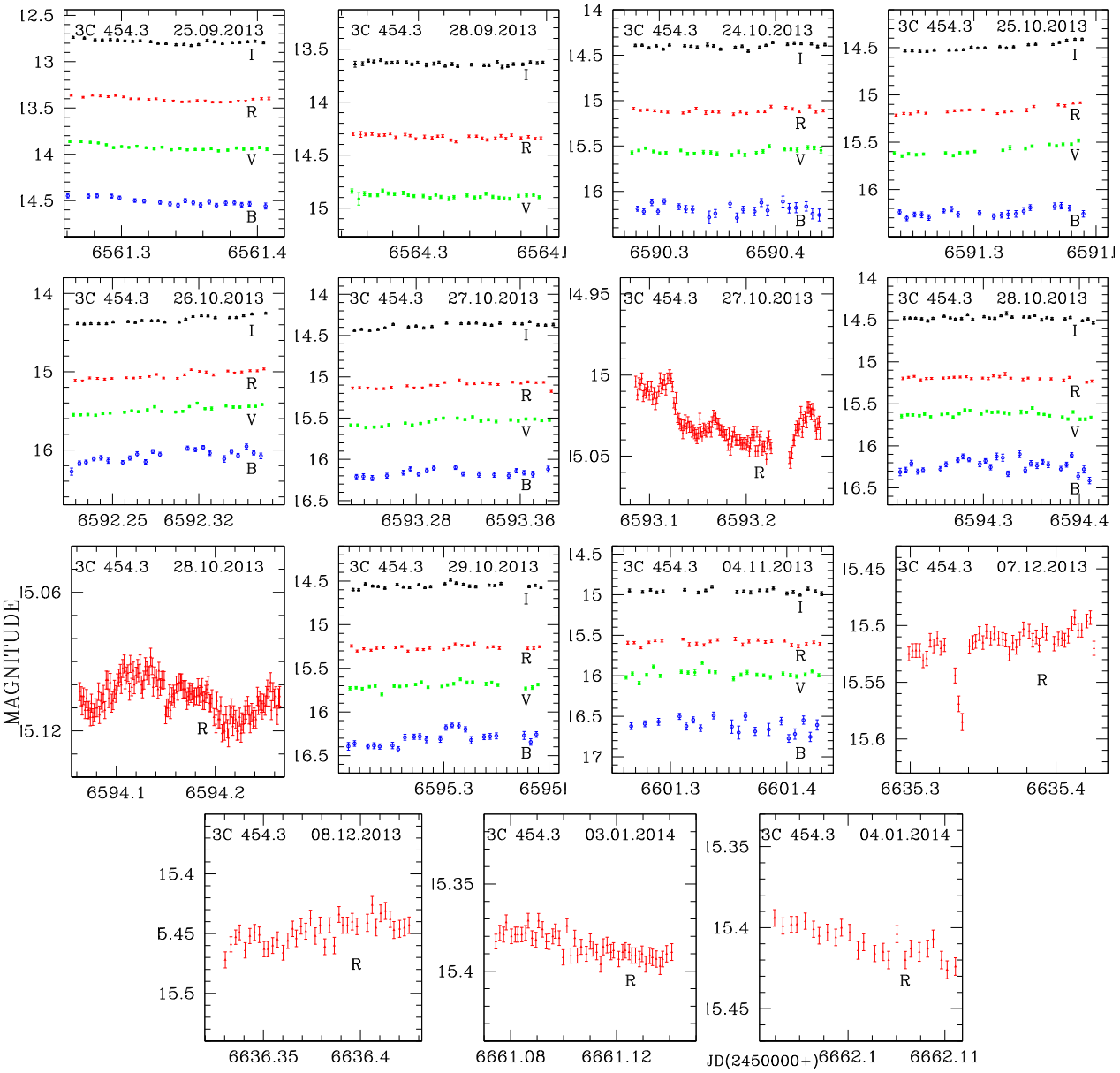

Figure 1. Light curves for 3C 454.3; open circles denote *B* filter LC; filled circles, *V* filter; filled triangles, *R* filter; open triangles, *I* filter. In each plot, X and Y axes are the JD and magnitude, respectively. Source name and observation date are indicated in each panel.

3.2 Structure function analysis

The first-order structure function (SF), introduced by Simonetti, Cordes & Heeschen (1985), is applied to each of the non-uniformly sampled LCs. The SF is designed to search for characteristic variability time-scales and possible periodicities. For details about SF as we have employed it, see Gaur et al. (2010).

The first-order SF initially increases with larger time lags but can indicate the following behaviours at larger lags: (1) a continuing rise with lag indicates that any characteristic time-scale of variability is longer than the length of the data set, with the longest time lag giving the minimum value of the time-scale of uncorrelated data points; (2) uncorrelated data produce a 'white noise' behaviour, characterized by a constant slope (Ciprini et al. 2003); (3) the presence of a plateau indicates a characteristic time-scale of the variability; (4) if the SF curve falls, producing a dip, after reaching a plateau, then the time lag at that local minimum value of the SF may mark the presence of a periodic cycle and this possibility is strengthened if there is a lag corresponding to differences between two or more minima; however, a single dip is considered spurious if observed at time lag close to the length of data run; (5) a very irregular SF is observed for variations dominated by one or few large outbursts or variations that are more or less periodic.

As pointed by Emmanoulopoulos, McHardy & Uttley (2010), the SF method sometimes leads to spurious results and thus incorrect claims of periodicities or time-scales. Hence we have also examined the data for time-scales and possible periodicities by the discrete correlation function (DCF) method.

3.3 Discrete correlation function (DCF)

The DCF technique, first presented by Edelson & Krolik (1988), is similar to the classical cross-correlation with an added advantage

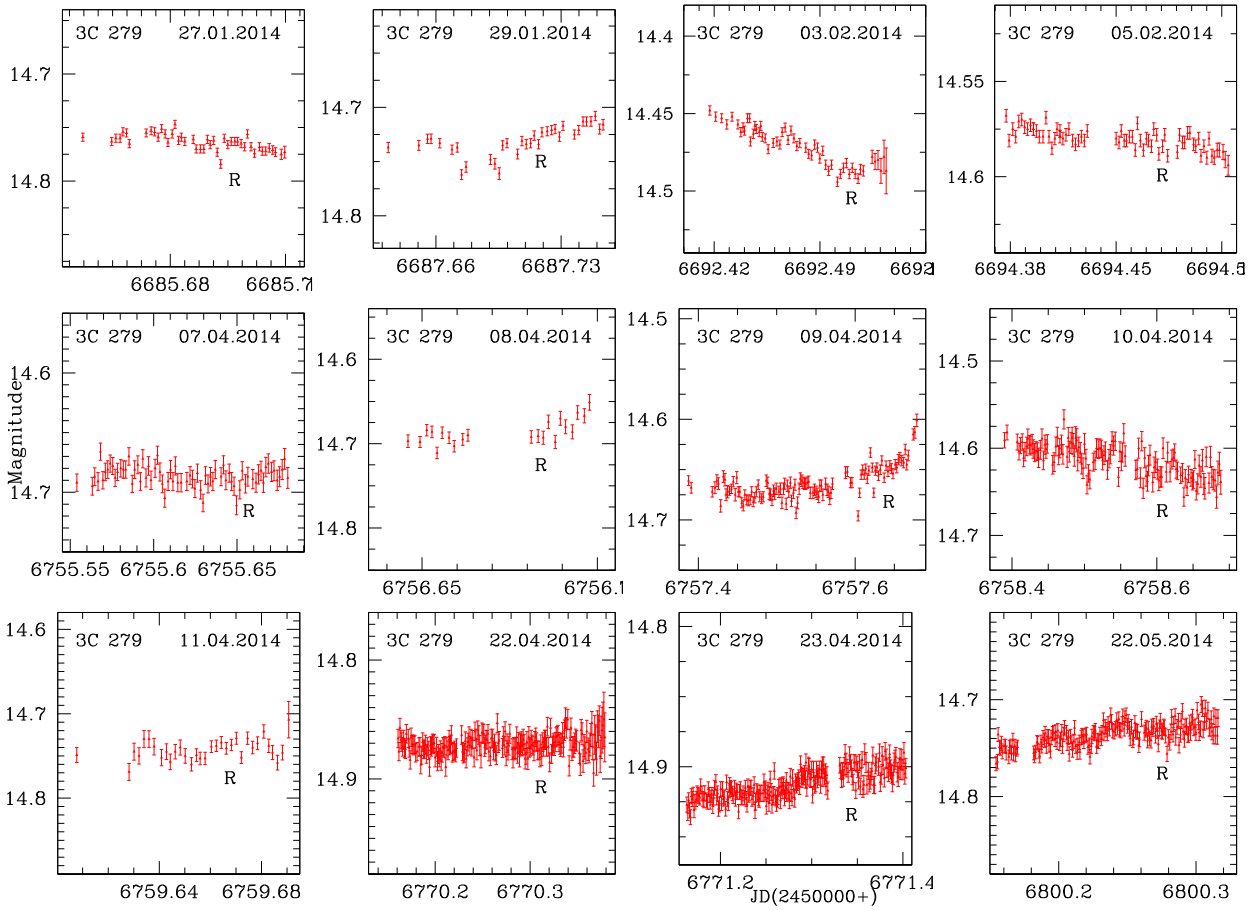

Figure 2. IDV LCs for 3C 279 with details same as in Fig. 1.

of being able to be used for the analysis of unevenly sampled data without interpolating data points, thus giving a meaningful estimation of the errors. Hufnagel & Bregman (1992) further generalized the method to include a better error estimate. In general, a DCF value >0 implies the two data signals are correlated, while the two anticorrelated data sets have a DCF < 0, and a DCF value equal to 0 implies no correlation exists between the two data trains. For quantitative details about the DCF see Agarwal & Gupta (2015), and references therein.

4 RESULTS

4.1 3C 454.3

3C 454.3 (PKS 2251+158) ($\alpha_{2000.0} = 22^{\rm h}53^{\rm m}57\overset{\rm s}{.}75$, $\delta_{2000.0} = +16^{\circ}08'53\overset{''}{.}56$) is a well-known FSRQ at a redshift of $z = 0.859$. It has displayed quite high optical activity since 2001 that has been suggested to be, at least in part, due to changes in the viewing angle caused by a helical jet geometry (e.g. Villata & Raiteri 1999; Raiteri et al. 2008). A significant increase in activity at optical and radio wavelengths in conjunction with multiple γ-ray flaring events detected with the *AGILE* and *Fermi* γ-ray satellites, renders 3C 454.3 well suited for multiwavelength campaigns (e.g. Fuhrmann et al. 2006; Pacciani et al. 2010).

In May 2005, a dramatic outburst was recorded in the radio to X-ray energy bands (e.g. Vercellone et al. 2010), reaching $R \approx 12$ mag before decaying to $R = 15.8$ mag in ∼75d (Villata et al. 2006). Based on the continuous monitoring of the object with the Whole Earth Blazar Telescope (WEBT) a quiescent state was reported during spring 2006–2007, which revealed the 'big blue bump' in the optical spectrum (a feature more typical of radio-quiet AGN), indicating thermal emissions from the accretion disc, as well as a 'little blue bump' due to line emission from the broad-line region (BLR) of the AGN (Raiteri et al. 2007). After this faint state the object again underwent multifrequency flaring activity in 2007 July (Vercellone et al. 2008) followed by multiple flares during 2007 November–December, reaching optical levels of $R = 12.69$ mag (Zhai, Zheng & Wei 2011). The 2010 October–December outburst extended over all wavelengths with γ-ray flux peaking at 85×10^{-6} photon cm^{-2} s^{-1} and optical emissions increasing simultaneously (Vercellone et al. 2011) as observed at several observatories (Larionov, Villata & Raiteri 2010; Semkov et al. 2010; Raiteri et al. 2011), along with increases in X-ray and radio fluxes (Wehrle et al. 2012; Jorstad et al. 2013).

Extensive flux variability observations at different frequencies over many years encouraged detailed modelling and analysis of SEDs which helped to interpret the physical conditions of the jet and the emission mechanism responsible for the emitted radiation (e.g. Finke & Dermer 2010; Böttcher et al. 2013).

4.1.1 *Intraday variability*

Our observations of 3C 454.3 were carried out on 13 nights spanning the period between 2013 September and 2014 January, to search for variability on intraday time-scales. The LCs of the blazar are displayed in Fig. 1. Photometric observations in the *B*, *V*, *R*, and *I* bands

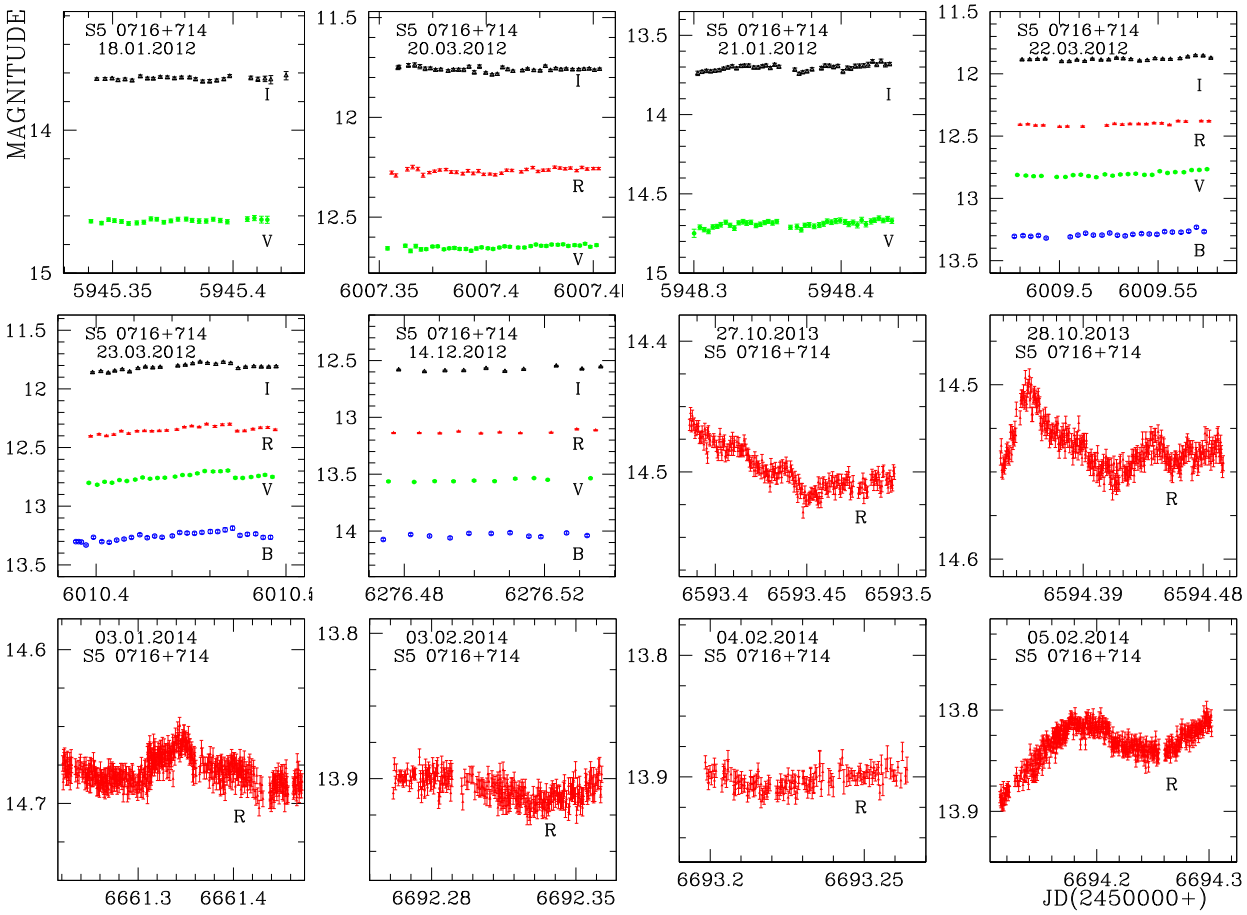

Figure 3. As in Fig. 1 for S5 0716+714.

were carried out essentially continuously and quasi-simultaneously on 2013 September 25, 28, October 24–29, and November 04 for a span of ∼4 h each. Also photometric observations only in the *R* band were carried out on 2013 October 27, 28, December 7, 8, and 2014 January 3, 4 for a span of ∼4 h each. We have labelled the plots with the blazar name and the date of monitoring. In order to claim the presence or absence of variability during the observations, we have used the *F*-test, at 0.99 confidence level, with results summarized in Table 2 whose complete version is presented in the supplementary materials online. Also, the details of the brightness changes in the source during the intranight optical variability (INOV) observations are listed in Table 3.

B passband: the target was observed in the *B* passband on eight nights for ∼4 h on an average. The *F*-test indicates that the source was variable in the *B* band on three nights: 2013 October 25, 28, and 29. During these eight nights the *B*-band brightness decayed to $B = 16.78$ mag which is ∼3.01 mag fainter than the brightest *B* magnitude level of 13.77 reported by Zhai et al. (2011). Hence the source might be best characterized as being in a post-outburst state during our observations of 2013. Recently, 3C 454.3 showed drastic increase in brightness reaching *B*-band magnitude of 14.14 on 2014 June 24. It decreased in brightness after then.

V passband: our *V* filter observations of 3C 454.3 lasted for a total of nine nights over spans of ∼4 h on each night. *C*-test results reveal the lack of microvariability in the source in the *V* band. The *F*-test results also support the absence of microvariability.

R passband: we monitored the blazar in *R* passband for 13 nights from 2013 September 25 through 2014 January 04, with duration ranging from 3 to 4 h. We detected noticeable variability on 4 out of these 13 nights: 2013 October 28, December 07, 08, and 2014 January 04. The *C* values for above dates indicate that the source is variable on 2013 December 07 with amplitude of variability reaching 9.16 per cent as the source changed in brightness from 15.525 to 15.520 mag in ∼3.1 h with a prominent dip observed at UT 14.57 h when it faded to 15.58 mag. On this night, the maximum variation noticed was $\Delta R \sim 0.1$ with the brightest level of 15.49 mag and faintest level at 15.58 mag. Analysis using the *F*-test indicates the presence of microvariability on the remainder of the observation dates mentioned above. During the span of 13 nights, we found that the target faded to $R = 15.40$ mag on 2014 January 14, which is ∼3.4 mag fainter than the brightest magnitude of $R \sim 12$ mag, as reported by Villata et al. (2006), but is still brighter by ∼1.6 mag than the faintest level of 17 mag. So, as noted for the *B* band, the FSRQ appears to be in a post-outburst stage during the later months of 2013. But during the flaring state of 2014 May it reached the brightest *R*-band magnitude of 13.143 on 2014 June 24.

I passband: we carried out monitoring observations of 3C 454.3 in the *I* band for nine nights between 2013 September 25 and November 11. The *C* values reveal the lack of microvariability in the source in the *I* band. The *F*-test results also support the absence of microvariability in *I*.

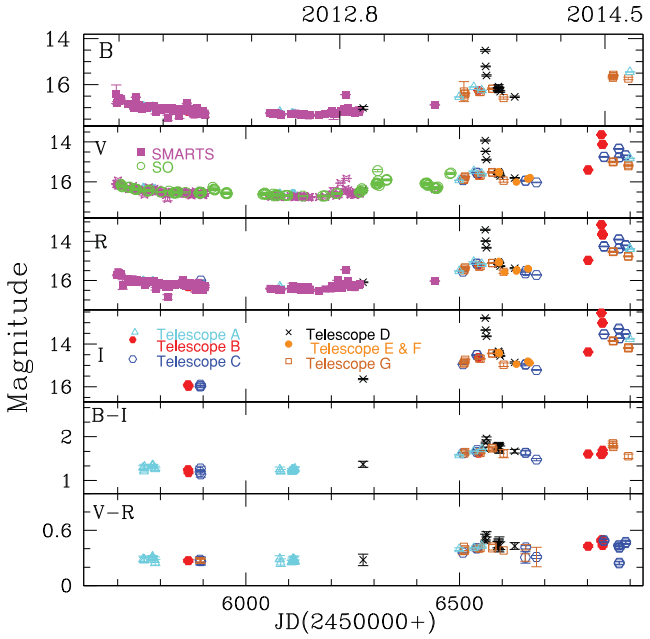

Figure 4. Short/long-term variability LCs and colour indices of 3C 454.3 in the *B*, *V*, *R*, and *I* bands and (*B*−*I*) and (*V*−*R*) colours. Different colours denote data from different observatories: cyan = telescope A, red = telescope B, blue = telescope C, black = telescope D, dark orange = telescopes E and F, chocolate = telescope G, magenta = SMARTS, green = SO.

4.1.2 Short-term and long-term flux variability

The STV/LTV LCs of 3C 454.3 in the *B*, *V*, *R*, and *I* passbands are shown in Fig. 4 along with the colour variations (*B*−*I*) and (*V*−*R*). For a particular date the magnitude is taken to be the mean magnitude of all image frames in a specific passband and the time is taken as the Julian Date (JD) value at UT = 00 h on the same date. For calculating the amplitude of variability using equation (3), we considered every data point available to us. Also, the details of the magnitude changes during the whole observation period are listed in Table 4.

B passband: the top panel of the figure shows the STV/LTV LC of 3C 454.3 in the *B* band; it includes our data along with those provided by SMARTS. We have monitored the source in *B* band for STV studies from JD 245 5620 to 245 6930 using the seven different telescopes described in Section 2 and indicated in the figure, which shows that after constantly decreasing in brightness, the source attained the faintest level on JD 245 4986.5, followed by a brightening trend till JD 245 5510.5. Since then the target decreased in brightness, displaying a maximum magnitude variation of ∼3.181. The same trends were noted by other authors (e.g. Zhai et al. 2011). The source showed increase in brightness during mid-year 2014. During the total time span, the amplitude of variability in the *B* band was calculated to be 318 per cent.

V passband: the corresponding STV/LTV LC in the *V* band is generated using our data along with that provided by SMARTS and SO, covering the time period between JD 245 4662.5 and 245 6930. After constantly decreasing in brightness since JD 245 5816.5, it recently entered a flaring stage reaching a minimum value of *V*-band magnitude on 2014 June 23. We found the amplitude of variability in *V* band to be ∼306 per cent.

R passband: The STV/LTV LC in the *R* band is displayed in the third panel from top in Fig. 4, which includes observations from SMARTS in addition to our data, and runs from JD 245 5759.5 to JD 245 6930. The object attained a large flux state of $R = 13.170$ mag on 245 5519.5. Zhai et al. (2011) have also reported the *B*- and *R*-band magnitudes of the source to be ∼14 and ∼13, respectively, in 2010 November, when the source was in a remarkably bright state. Since then the brightness of 3C 454.3 generally has been declining. It seems to have entered the post outburst stage in 2013. As in the other bands, in mid-2014 there was an increase in the flux of the target. But we also saw it decreased in brightness reaching an *R*-band magnitude of 14.38 on JD 245 6899.5. The amplitude of variability was found to be as large as ∼362 per cent.

I passband: the third panel from the bottom in above-mentioned figure represents the *I*-band LC during observations made between JD 245 5759.5 and 245 6930. We calculated the variability amplitude to be 320 per cent using equation (3).

4.1.3 Colour variability on diverse time-scales

We have investigated the variations of the (*B*−*V*), (*B*−*I*), (*V*−*R*), and (*R*−*I*) colours on intraday time-scales and presented the results

Table 4. Results for STV/LTV studies displaying magnitude changes in each band.

Source	Band	Faintest mag	JD (Max)	Brightest mag	JD (Min)	Δm
3C 4543.3	*B*	17.47	245 4986.5	14.14	245 6832.5	3.33
	V	16.84	245 5816.5	13.63	245 6832.5	3.21
	R	16.85	245 5816.5	13.14	245 6832.5	3.71
	I	16.07	245 6108.5	12.55	245 6832.5	3.52
3C 279	*B*	18.77	245 5316.7	15.10	245 6721.8	3.67
	V	18.25	245 5314.6	14.62	245 6721.8	3.63
	R	17.70	245 5400.5	14.12	245 6721.5	3.56
	I	14.30	245 6771.1	13.84	245 6692.4	0.46
S5 0716+714	*B*	15.72	245 6662.1	13.13	245 6007.3	2.59
	V	15.70	245 6662.1	12.60	245 6011.7	3.12
	R	14.70	245 6661.4	12.28	245 6007.4	2.42
	I	14.11	245 6662.1	11.75	245 6007.4	2.36

Notes. Column 1 is the source name, column 2 indicates the band in which observations were taken, column 3 represents the maximum magnitude attained by the source in the filter mentioned in previous column on a particular JD which is given in column 4, followed by minimum magnitude value and respective JD in column 5 and column 6 and finally the net magnitude change during IDV observations is given in column 7.

in Table 2. Performing *C*- and *F*-test on each night's data sets allowed us to quantify that the source rarely showed significant colour variations: according to the *F*-test, colour variability was detected on three nights, namely 2013 October 25, 28, and 29.

In Fig. 4 , we have shown the $(B-I)$ and $(V-R)$ colour indices as functions of time in the second and first panels from the bottom, respectively. The plots indicate moderate colour variations in both of these indices. The maximum variation seen in the source in $(V-R)$ is 0.308 mag found between 0.249 mag at JD 245 6081.5 and 0.557 mag at JD 245 6563.5. In the $(B-I)$ colour index the maximum variation noticed during our observation span was found to be 0.820 between the colour index values of 1.963 mag at JD 245 6563.5 and 1.143 mag at JD 245 5894.5.

4.2 3C 279

The FSRQ 3C 279 ($\alpha_{2000.0} = 12^{\rm h}56^{\rm m}11\overset{\rm s}{.}17$, $\delta_{2000.0} = -05^{\circ}47'21\overset{''}{.}5$) at a redshift of 0.536 (Burbidge & Rosenberg 1965) displays violent flux variability in all wavelength bands. It has been intensively studied through several simultaneous multiwavelength campaigns (e.g. Hartman et al. 1996; Wehrle et al. 1998; Böttcher et al. 2007). The source has been regularly variable in optical bands with very large optical variation of $\Delta B > 6.7$ mag (ranging between 11.3 and 18.0; Netzer et al. 1994) from the archival plates of the Harvard collection as reported long ago by Eachus & Liller (1975). A large amplitude STV of $\Delta R = 1.5$ mag was reported in 42 d (Gupta et al. 2008a).

During a 2006 WEBT campaign a dramatic flare was reported at radio, NIR, and optical frequencies with $R \sim 14.0$–14.5 mag. Quasi-exponential decays of *B*, *V*, *R*, and *I* fluxes of ∼1 mag on a time-scale of ∼12.8d, between JD 245 3743 and JD 245 3760, was displayed by the source (Böttcher et al. 2007), which prompted Böttcher & Principe (2009) to propose this being a signature of deceleration of a synchrotron emitting jet component.

The SED of 3C 279 has two broad peaks believed to be associated with synchrotron and inverse Compton emission. The 'Compton hump' can be explained by the synchrotron self Compton (SSC) process through the cooling of a relativistic electron distribution. But, since it requires extremely low magnetic field (Böttcher, Reimer & Marscher 2009) and high radiation energy density in comparison to the magnetic energy density (Maraschi, Ghisellini & Celotti 1992), it poses problems in explaining the very high energy (VHE) emission. So another explanation is the external Compton mechanism where the target photons from the accretion disc, or BLR clouds, or dusty torus are strongly deboosted.

4.2.1 *Intraday variability*

R passband: we carried out our photometric observations of 3C 279 during the period 2014 January–May for IDV studies in the *R* passband, for a total of 12 nights. The extracted LCs are displayed in Fig. 2. The details of magnitude changes on intraday basis during the 12 nights are given in Table 3. Gupta et al. (2008a) reported the source to be in the outburst state with $R \sim 12.6$ mag. During our last observations the FSRQ seems to be in somewhat of a post-outburst state with *R*-band magnitude of 14.75 as on 2014 May 24. It was found to be variable with continuous, but small decreases, in magnitude until it again flared in 2014 May. So 3C 279 was found to be highly variable during the IDV observations and seems to be in an active, if not outburst, state.

4.2.2 *Short-term and long-term flux variability*

The STV/LTV LCs of 3C 279 are displayed in Fig. 5 in *B*, *V*, *R*, and *I* filters which includes our *B*, *V*, *R*, and *I* data points along with the SMARTS (in *B*, *V*, *R*) and SO (in *V* passband only) data points covering the time interval from JD 245 4480 to JD 245 6900. The colour variation $(B-I)$ and $(V-R)$ are also displayed in Fig. 5 lower two panels. Also, the details of the magnitude changes during the whole observation period are listed in Table 4 for each passband.

B passband: STV/LTV LCs of the source in *B* band includes our data along with those provided by SMARTS and is plotted in the topmost panel of Fig. 5. The source has recently been found to be in a flaring state, with the brightest *B* magnitude in last 5 yr noted as 15.101 on 2014 March 05. Thus it is still 3.8 mag fainter than the 1936–1937 outburst, which is the classic outburst used for comparison, when it reached B ∼11.3. The target has been highly variable on yearly basis with LTV amplitude to be 338 per cent, during the ∼5 yr period.

V passband: the photometric observations of 3C 279 in *V* band includes our data from seven telescopes mentioned in Table 1 along with SMARTS data sets and supplemented with the data from SO. The STV/LTV LCs for *V* filter are shown in Fig. 5 where different colours refer to different telescopes, as listed in the caption. Recently, the source was noted to show a rapid brightness increase reaching the brightest level on 2014 March 5. The STV/LTV amplitude in *V* passband was calculated to be 338 per cent. The source was found to undergo small decrease in brightness with $V = 15.15$ on 2014 May 24 (JD 245 6802.175).

R passband: the STV/LTV *R*-band LC plotted in Fig. 5 is comprised of data from seven telescopes along with data sets obtained from SMARTS. The source was found to be in high state during 2014. We calculated the amplitude of variation to be 263.6 per cent.

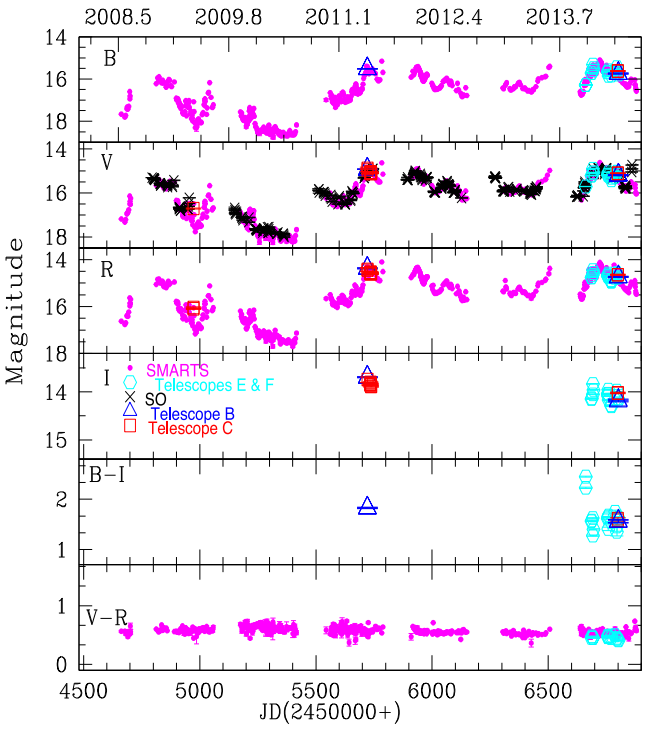

Figure 5. Short/long-term variability LCs and colour indices of 3C 279 in the *B*, *V*, *R*, and *I* bands and $(B-I)$ and $(V-R)$ colours. Different colours denote data from different observatories: magenta, SMARTS; cyan, telescopes E and F; blue, telescope B; red, telescope C; black, Seward.

The source was highly variable during last 5 yr and seems to be in an active stage presently.

I passband: 3C 279 was observed in *I* band for STV/LTV purpose using the seven telescopes mentioned in Table 1. There were no data points from SMARTS in the *I* passband. The last data point taken by us in this band was on 2014 May 24 when the source was found to have $I = 14.2$; this still corresponds to a bright state. The amplitude of variability calculated for the source during our shorter span of observations reached only 43.2 per cent.

4.2.3 Colour variability

We have also examined the colour variability in the source on short-term basis and this is displayed in the bottom two panels of Fig. 5. The maximum difference in the $(V-R)$ colour for 3C 279 is 0.85 mag (between its colour range 0.29 and 1.14 mag) while for $(B-I)$ difference was of 1.173 mag when maximum colour difference was 2.45 and minimum being 1.277.

4.3 S5 0716+714

The high declination ($\alpha_{2000.0} = 07^{\rm h}21^{\rm m}53\overset{\rm s}{.}4$, $\delta_{2000.0} = +71^{\circ}20'36\overset{''}{.}4$) BL Lac is one of the most well-studied objects over entire EM spectrum and is an extremely variable source on diverse time-scales, ranging from minutes to years (Heidt & Wagner 1996; Nesci et al. 1998; Giommi et al. 1999; Raiteri et al. 1999; Gupta et al. 2008a,b). S5 0716+714 is one of the most active and bright BL Lacs in the optical bands with a featureless optical–UV continuum (Biermann et al. 1981; Hartman et al. 1999) thus making it very hard to estimate the redshift. Nilsson et al. (2008) determined the redshift of the source to be 0.31 ± 0.08 using the marginally detected host galaxy as the standard candle plus its location close to three galaxies of redshifts 0.26 (Bychkova et al. 2006). In the past, S5 0716+714 has been found to have duty cycle of 1 (Wagner & Witzel 1995) implying the source to be always in active state and hence has been extensively observed on IDV time-scales (e.g. Montagni et al. 2006; Gupta et al 2008a,b and references therein) covering five major optical outbursts with an interval of $\sim 3.0 \pm 0.3$ yr (e.g. Gupta et al 2008a).

Gupta, Srivastava & Wiita (2009) used wavelet analysis to analyse the archived optical data of the source obtained by Montagni et al. (2006) and found quasi-periodic oscillation (QPO) components ranging between ∼25 and ∼73 min on several nights. Later, a QPO of ∼15 min was reported by Rani et al. (2010b) at optical frequencies. Quirrenbach et al. (1991) claimed a possible QPO of ∼1 d in optical and radio bands simultaneously.

4.3.1 Intraday variability

We observed S5 0716+714 on 12 nights between 2012 January and 2014 February, to search for IDV in multiband fluxes. The calibrated LCs of the blazar are displayed in Fig. 3. To search and analyse blazar variability, we have employed the *C*- and *F*-test, as discussed in Section 3.1. The brightness changes on intraday basis during the 12 nights are given in Table 3 in each particular filter.

B passband: the source was observed in the *B* filter on three nights for ∼4 h on average. Following *F*-test we found the source to be variable on March 23 with amplitude of variability reaching a maximum of ∼13.5 per cent.

V passband: our *V* passband observations of the target were carried out for six nights (2012 January 18, 21, March 20, 22, 23, and December 14). Using *F*-test the source was found to be variable on January 21 and March 23 when their variation exceeded 0.99 significance level with amplitude of variability reaching 11.17 per cent.

R passband: the BL Lac's monitoring in the *R* filter for 10 nights spans the period from 2012 March to 2014 February with ∼4 h average on each night. On six of these nights the variations exceeded 0.99 significance, with amplitude of variability reaching a maximum of ∼9.5 per cent on 2012 March 23. During those nights, the source was found to be in an active state.

I passband: this source was monitored in *I* passband for a span of about 6 d occurring on 2012 January 18, 21, March 20, 22, 23, and December 14. We tested for IDV using both tests. Using the *F*-test we found that the source showed significance levels above 99 per cent for microvariability on two nights, 2012 January 01 and March 03. During our observations, the maximum amplitude of variability went up to ∼8.5 per cent by 2012 March 23.

4.3.2 Short-term and long-term flux variability

We investigated the BL Lac in *B*, *V*, *R*, and *I* filters during the period between JD 245 4743.95 454 and JD 245 6804.65 226 to study optical properties corresponding to short-term flux-variability. These LC plots are displayed in Fig. 6 along with the colour variation LCs of $(B-I)$ and $(V-R)$ in different panels. Also, the details of the magnitude changes during the whole observation period are listed in Table 4 for each passband.

B passband: the STV/LTV LC of S5 0716+714 in the *B* passband is displayed in the upper panel of the figure where we used the data from the seven telescopes mentioned in Table 1, observed between the above-mentioned period. We calculated variability amplitude of ∼225 per cent in *B* band.

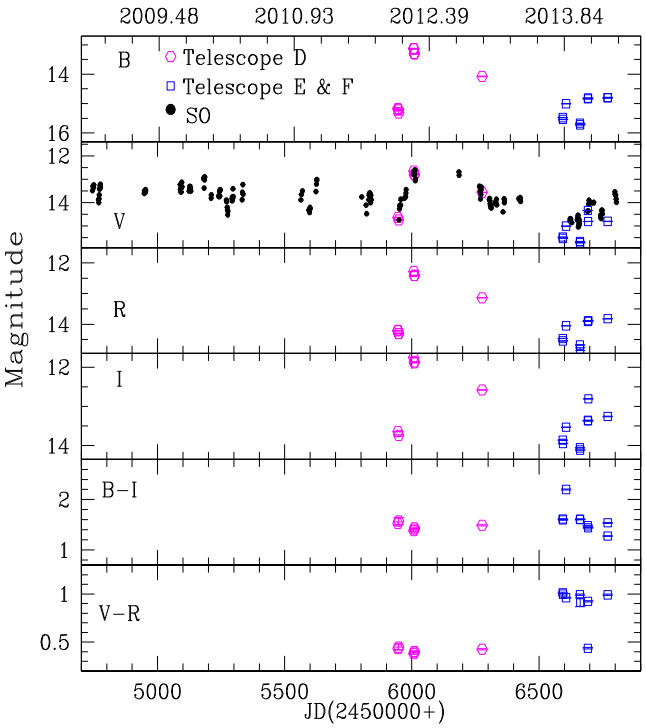

Figure 6. Short/long-term variability LCs and colour indices of S5 0716+714 in the *B*, *V*, *R*, and *I* bands and $(B-I)$ and $(V-R)$ colours. Different colours denote data from different observatories: magenta, D; blue, telescopes E and F; black, SO.

V passband: the STV/LTV LC of the source in the *V* passband is displayed in the second panel from the top of the above-mentioned figure with our data points using the seven telescopes mentioned in Table 1 and the data from SO. We calculated the variability amplitude using equation (3) and found that the source varied by 306 per cent.

R passband: the LC for -term studies of the source in *R* band is generated using the data taken from the seven optical telescopes mentioned in Table 1. The variability amplitude was calculated to be ∼240 per cent in *R* band.

I passband: the corresponding LC for *I* band is displayed in the third panel from the bottom of the above figure where data used is taken from the seven optical telescopes mentioned in Table 1. The maximum variation noticed in the target is 2.361 with STV/LTV amplitude of ∼221 per cent in *I* band.

4.3.3 *Colour variability*

The maximum variation noticed in the target for (*B*−*I*) is 0.817 (between its colour range 1.382 mag on JD 245 6007.3 and 2.199 mag on JD 245 6694.3) while for (*V*−*R*) is 0.634 (between its colour range 0.379 mag on JD 245 6007.3 and 1.013 mag on JD 245 6593.4).

5 CROSS-CORRELATED VARIABILITY

To search for and quantify any possible correlations between the optical fluxes we used the DCF technique, as explained in Section 3.3. We searched for possible time lags, which could be used to probe physical conditions in the inner regions of AGNs. The shortest possible time-scale of variability is normally associated with the changes occurring in jet-emitting region, whose time-scales are shortened by Doppler beaming..

For 3C 454.3, on most of the nights the DCFs between the LCs in different optical bands peak at small time lags ranging from 0 to 0.07 h which cannot be considered significant as these time lags are close to the measurement intervals or might be due to photometric and systematic errors on individual data points of both LCs. According to White & Peterson (1994) and Peterson et al. (1998), any detection of time lags is limited to lags longer than the LC sampling time-scale, which prevents us from measuring time lags on time-scales less than a few minutes. In order to further investigate this issue we performed a SF analysis to see if there was a discernable time-scale of variability by following the description given in Section 3.2. This SF approach indicated that any time-scale of variability is greater than or close to the total length of our observations, and therefore not reliable. Also, any nominally positive SF results were not supported by the DCF results. We therefore conclude that our observations did not reveal any characteristic time-scale of variability or any time delays among the various optical bandpasses. The small frequency intervals in the optical regime lead to null or small time lags which implies that the photons in these wavebands are emitting by the same physical process and from the same emitting region.

For the FSRQ 3C 279, the SF for the *R*-band LC on January 29 gives a hint of variability at 72 min from both SF and DCF analysis, but it is likely to arise from gaps in the LC. After that nothing significant is seen on 2014 February 3 and 5. For rest of the *R*-band LCs of 3C 279 we do not find any time-scale of variability as the shape of the SF indicates that any time-scale of variability that might be present is greater than the length of our observation. Plots are given in the online-only material.

From the SF evaluation of S5 0716+714 for the LC of 2012 January 21 in *I* and *V* bands, we get a possible time-scale of variability ∼1.2 h in both the bands, which is to some extent supported by the DCF also. On March 23 we observed the source in *B*, *V*, *R*, and *I*. The SF and DCF for *R*-band LC indicate a variability time-scale of 1.44 h, while for the *B*, *V*, and *I* bands for the same day we get variability time-scales of 1.92, 1.44, and 1.44 h, respectively. The SF plot for the 2013 October 27 LC displays a continuous rising trend that indicates that any time-scale of variability exceeds the length of our observations. The nominal time-scale of variability for the LC observed on 2014 January 03 is found to be 2.4 h which is also supported by DCF analysis. Moving on to 2014 February, we see that the *R*-band LCs taken on February 3 show a possibility of IDV time-scale of 1.44 h from the SF analysis which is supported by DCF technique also. Whereas on February 4 and 5 we see a continuous rising trend followed by a dip, thus giving possible variability time-scales of 72 and 86.4 min from both SF/DCF approaches. The SF and DCF plots for the target are displayed in the supplementary material while a sample of the same is given in Fig. 7.

6 COLOUR–MAGNITUDE RELATIONSHIP

In this section we investigate any relationship between the optical variations in the (*B*−*V*), (*V*−*R*), (*R*−*I*), and (*B*−*I*) colour indices of the source and the brightness variations, which can be used to study colour behaviour and variability scenarios.

The colour–magnitude plots for the nine nights in the case of 3C 454.3 (i.e. 2013 September 25, 28, October 24–29, November 04) and six nights for S5 0716+714 (i.e. 2012 January 18, 21,

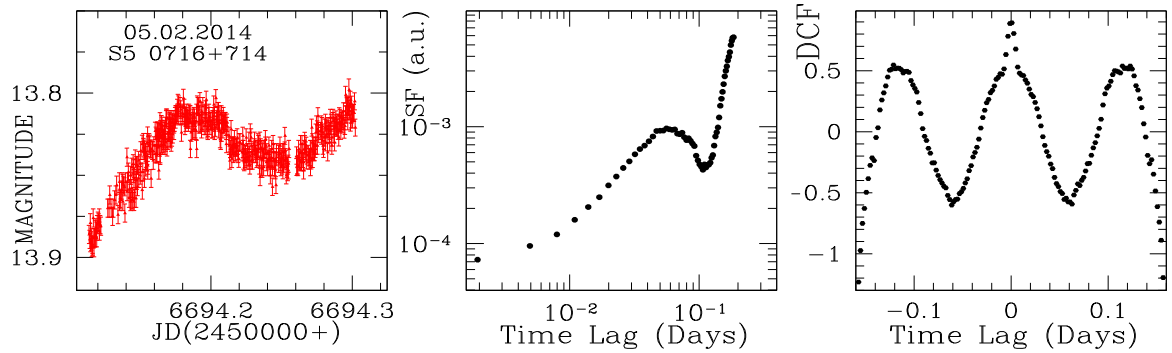

Figure 7. *R*-band optical IDV LC of the blazar S5 0716+714 and their respective SFs and DCFs. The remainder of these observations and analyses are presented as online-only material.

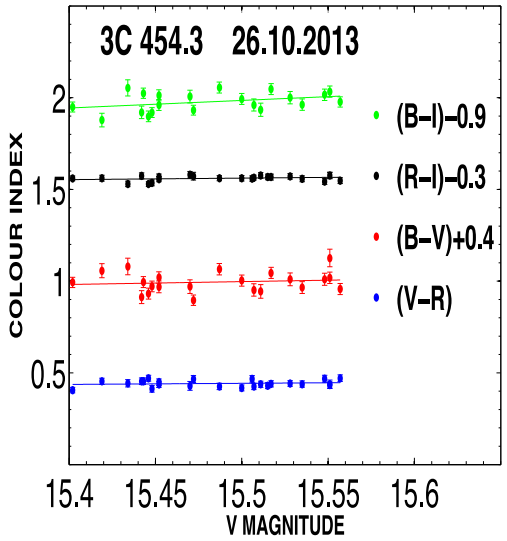

Figure 8. Colour–magnitude plots on intraday time-scales for 3C 454.3. The *V* magnitudes are given on the X-axis and the various labelled colour indices are plotted against them for each labelled date of observation. Colour–magnitude plots for remaining observation dates are available online.

March 20, 22, 23, and December 14) are displayed in the Supporting Information section while a sample of the same is displayed in Fig. 8. Colour variation behaviours in blazars are still a topic of debate. A bluer-when-brighter (BWB) trend is commonly observed in blazars (e.g. Clements & Carini 2001; Raiteri et al. 2001; Villata et al. 2002; Papadakis et al. 2003; Papadakis, Villata & Raiteri 2007; Rani et al. 2010a; Agarwal & Gupta 2015), in particular those of the HSP class, in which the optical continuum is generally believed to be entirely dominated by the non-thermal jet synchrotron emission. In LSP blazars, in which the accretion disc can provide a substantial contribution to the optical continuum, a redder-when-brighter (RWB) trend sometimes indicates the increasing thermal contribution at the blue end of the spectrum, with decreasing non-thermal jet emission (e.g. Miller 1981; Villata et al. 2006; Raiteri et al. 2007; Gaur, Gupta & Wiita 2012). For each night, we have calculated a linear fit of the colour indices, CI, against *V* magnitude: CI $=mV + c$. The corresponding fit values of the slope, m, and the constant, c, are reported in Table 5. The linear Pearson correlation coefficient, r, and the corresponding null hypothesis probability, p, are also reported there. A positive slope indicates a positive correlation between the colour indices and apparent magnitude of the blazar which implies the general trend of BWB (or redder-when-fainter) whereas a negative correlation is observed for a negative slope, indicating an RWB behaviour.

For 3C 454.3, we found significant positive correlations ($p \leq 0.05$) between the *V* magnitude and most of the colour indices on almost all nights except on 2013 October 24 when the object exhibited a negative correlation. Thus, the BWB trend was prominent during our observations. That the spectrum steepens as the brightness decreases can be clearly seen in the plots of 2013 September 25 ($V-R$), September 28 ($V-R$), October 25 ($V-R$), October 27 ($V-R$), October 28 ($V-R$ and $B-I$), October 29 ($B-I$ and $V-R$), and November 04 ($V-R$). However, an RWB trend was found on October 24 ($B-V$ and $B-I$) when the spectrum becomes steeper as the source brightens, as evident from the plot. For other colours in the respective nights, no correlation above the 95 per cent

Table 5. Fits to colour–magnitude dependences and colour–magnitude correlation coefficients.

Source	Date of observation	$B-V$ versus V		$V-R$ versus V		$R-I$ versus V		$B-I$ versus V	
		m^a	c^a	m	c	m	c	m	c
		r^a	p^a	r	p	r	p	r	p
3C 454.3	25-09-2013	−0.043	1.487	0.322	−3.969	0.102	−0.203	0.302	−2.473
		−0.045	0.833	0.496	0.014	0.163	0.445	0.288	0.173
	28-09-2013	–	–	0.613	−8.568	0.099	−0.779	–	–
		–	–	0.577	0.001	0.010	0.613	–	–
	24-10-2013	−1.004	16.562	0.443	−6.442	−0.117	3.133	−1.049	16.953
		−0.462	0.030	0.594	0.003	−0.145	0.509	−0.488	0.040
	25-10-2013	−0.598	10.260	0.452	−6.611	−0.063	2.291	0.077	0.576
		−0.301	0.173	0.603	0.002	−0.15	0.580	0.039	0.862
	26-10-2013	0.156	−1.818	0.060	−0.482	0.082	0.292	0.414	−4.425
		0.132	0.559	0.150	0.484	0.258	0.234	0.367	0.102
	27-10-2013	−0.393	7.231	0.256	−2.438	0.078	−0.488	−0.153	4.170
		−0.026	0.106	0.565	0.005	0.153	0.497	−0.130	0.607
	28-10-2013	0.479	−6.574	0.799	−11.158	−0.032	0.918	1.020	−14.183
		0.249	0.202	0.849	0.00001	0.052	0.801	0.530	0.004
	29-10-2013	0.430	−5.640	0.759	−10.382	0.025	0.322	1.167	−16.576
		0.237	0.277	0.789	0.000	0.028	0.897	0.598	0.003
	04-11-2013	−0.733	12.352	0.840	−13.032	0.0481	−1.775	0.171	−1.068
		−0.338	0.157	0.763	0.0001	0.078	0.735	0.086	0.735
S5 0716 +714	20-03-2012	–	–	0.412	−4.829	0.602	−7.111	–	–
		–	–	0.334	0.046	0.422	0.010	–	–
	22-03-2012	−0.219	3.336	0.337	−3.912	0.228	−2.255	0.337	−3.509
		−0.300	0.165	0.579	0.007	0.466	0.038	0.490	0.018
	23-03-2012	−0.044	1.121	0.137	−1.350	0.110	−0.722	0.068	−0.030
		−0.107	0.626	0.476	0.016	0.373	0.072	0.159	0.468
	14-12-2012	−0.700	9.972	0.638	−8.227	−0.0344	1.019	−0.039	1.190
		−0.432	0.213	0.673	0.047	−0.0293	0.936	−0.022	0.952

Notes. [a] m = slope and c = intercept of CI against *V*; r = Pearson coefficient; p = null hypothesis probability.

confidence level was present. Thus the FSRQ showed multiple instances of positive correlations and one single instance of a negative correlation, along with several colour–magnitude sets showing no correlations at all. In general, the BWB trend was prominent during our observations.

According to Sasada et al. (2010), the colour–magnitude relationship varies among the outburst state, the active state, and the faint state. 3C 454.3 followed a BWB trend in the outburst state, whereas it exhibited an RWB trend in the faint state and again a BWB trend was associated with an active state. From Section 4, during the time span of our observations 3C 454.3 was ∼3.4 mag fainter than the brightest known magnitude of $R \sim 12$, but brighter by ∼1.6 mag than the faintest level of $R = 17$ mag. Hence it seems to be classified best as being in an active state (out of the three states above) and the colour behaviour obtained by us is consistent with those reported in Sasada et al. (2010) and Gu & Ai (2011), according to which the RWB trend is rarely seen for FSRQs.

Though usually dominated by jets, the optical emission of blazars is generally a combination of jet and accretion-disc photons. The optical emission from 3C 454.3 is possibly contaminated by thermal emission from the accretion disc, providing a slowly and weakly variable 'blue' emission component, which may make a substantial contribution to the blue–UV continuum, as FSRQs are usually low-frequency synchrotron peaked sources (e.g. Abdo et al. 2010). The BWB trend, prevailing when the jet synchrotron emission completely outshines the accretion-disc emission, can be explained through an episode of more efficient acceleration of relativistic particles in the jet. In a relatively simple model, this can be represented an injection of fresh electrons with an energy distribution harder than that of previous, partially cooled electrons (e.g. Kirk, Rieger & Mastichiadis 1998; Mastichiadis & Kirk 2002). More detailed simulations of such a scenario, based on the solution of a Fokker–Planck equation of the electron distribution including first- and second-order Fermi acceleration, have been done (e.g. Diltz & Böttcher 2014; Chen, Pohl & Böttcher 2015). The latter work has demonstrated that, if an increased level of optical synchrotron emission is caused by a temporary decrease of the stochastic particle acceleration time-scale, optical and (SSC dominated) X-ray emissions are expected to be anticorrelated, with the X-ray variations lagging behind the optical variations by several hours. Instead, Raiteri et al. (2011) found a good correlation with a delay of about 1 d. This is a prediction that could be tested with future, coordinated optical and X-ray monitoring observations of 3C 454.3.

We found significant positive correlation for S5 0716+714 e.g. on 2012 March 20 ($V-R$ and $R-I$), March 22 ($V-R$), ($R-I$) and ($B-I$), March 23 ($V-R$), and also on December 14 ($V-R$). No significant negative correlations are found, thus indicating that the BL Lac tends to be bluer (flatter) when brighter on time-scales of days, which may be due to the contribution of two components to the optical emission: one is the variable with a flatter slope (α_1) ($f_\nu \propto \nu^{-\alpha}$) and the second one being the stable one with $\alpha_{\rm const} > \alpha_1$. The BWB trend for this source was also given by Villata et al. (2000) during the 1999 WEBT campaign in a 72-h optical LC. In the case of BL Lacs, any colour changes owing to accretion disc are highly unlikely, as the disc radiation is overwhelmed by that from the Doppler-boosted jet emission. Therefore, shock-based jet models are most likely to explain the observed colour variations (e.g. Marscher & Gear 1985; Marscher et al. 2008), since radiation at higher frequencies is expected to emerge first followed by the flux at lower frequencies, thus producing a bluer colour during the early phase of a flare while a redder one appears during the later observation of the same flare, as it decays.

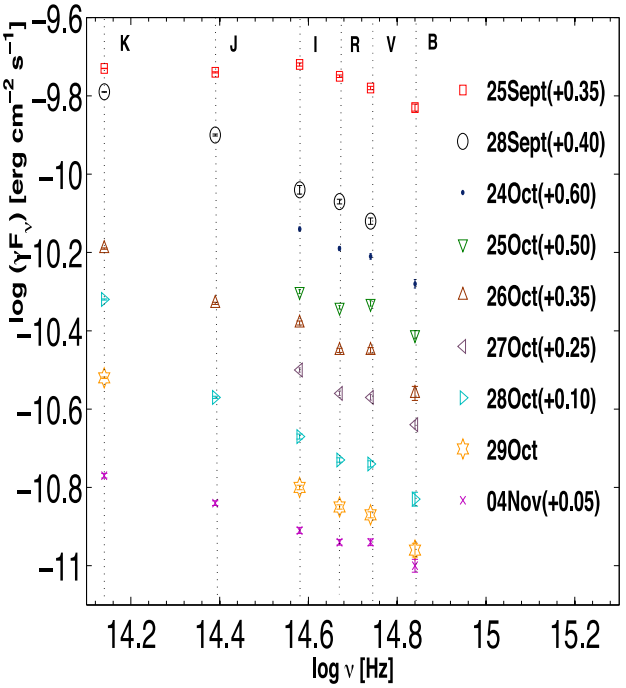

Figure 9. SED results for 3C 454.3 in NIR–optical frequency range.

7 SPECTRAL ENERGY DISTRIBUTIONS

SED properties of a source are an excellent way to investigate theoretical models. Since simultaneous multifrequency observations are difficult to attain, it is much simpler to focus on a narrow region of EM spectra like NIR/optical, which could provide vast amount of information on flux and spectral variability that in turn can provide evidence about the emitting regions of the relativistic electrons, constrain the γ-ray emission models (Ghisellini el al. 1997) and the contributions of emissions from jets (synchrotron), BLR, accretion disc, host galaxy, and surrounding regions.

Using our B, V, R, and I observations along with the J and K band data points for 3C 454.3 available on the SMARTS web page, for each particular night, we generated nine NIR–optical SEDs spanning 2013 September 25–November 04. For that purpose, we have subtracted Galactic extinction, A_λ, obtained from the NASA/IPAC Extragalactic Database[5] from the optical/NIR data points, to obtain extinction-corrected fluxes, which were then converted to νF_ν fluxes. The resulting SEDs are displayed in Fig. 9. From the figure it appears that a bump peaking in the $V-B$ frequency range is present in the lower-brightness optical SEDs. It most likely corresponds to the little blue bump observed in quasars in the rest wavelength range ∼200–400 nm for which the strong emission lines from the BLR seem to be responsible (e.g. Raiteri et al. 2007). As expected, this feature disappears in the two brightest SEDs. The brightest SED for 3C 454.3 was measured on 2013 September 25. Minor variations were seen in the SEDs for October 25–28 Oct after which it decayed day by day, reaching a minimum on 2013 November 4.

Fig. 10 shows the SED of 3C 279 during 2014 January–May covering NIR to optical. We selected 9 d when there were

[5] http://ned.ipac.caltech.edu

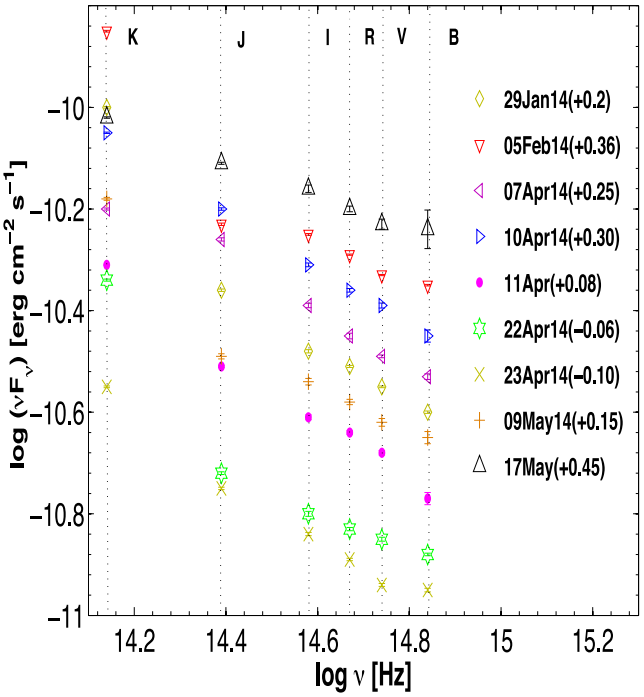

Figure 10. SED results for 3C 279 in NIR–optical frequency range.

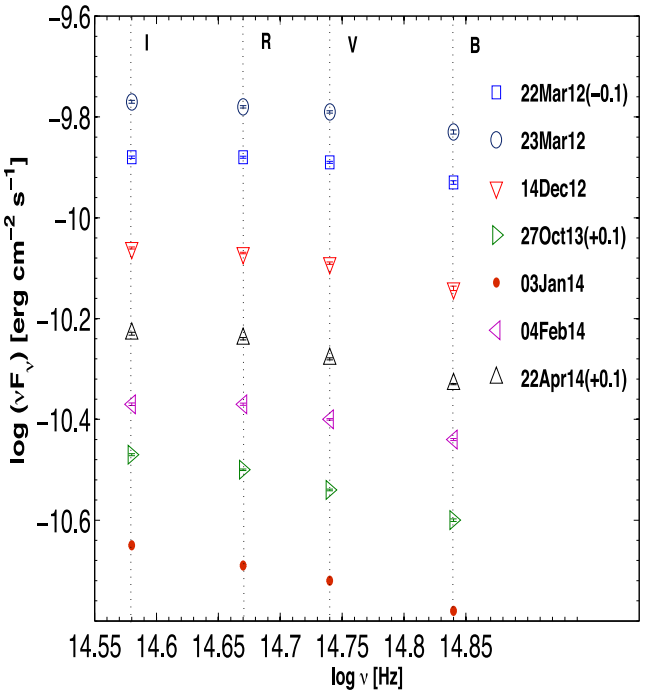

Figure 11. SED results for S5 0716+714 in optical frequencies.

quasi-simultaneous observations in *B*, *V*, *R*, *I*, *J*, and *K* to perform a limited spectral analysis of the source. The NIR and optical data have been corrected for Galactic extinction following Cardelli, Clayton & Mathis (1989) using total to selective extinction ratio $A_v/B_{B-V} = 3.1$ (Rieke & Lebofsky 1985). We find significant changes in NIR region. We apparently are seeing a signature of one of the broad bumps peaking in the NIR region, which should be the synchrotron component as it peaks in IR/optical bands in case of red blazars (located between $10^{12.5}$–$10^{14.5}$ Hz). We get the brightest and faintest SEDs for 2014 February 05 and April 23, respectively.

Fig. 11 shows optical–NIR SED for the source S5 0716+714, built with our *B*, *V*, *R*, *I* data sets for seven different epochs with different brightness levels. Magnitudes in all bands were corrected for Galactic extinction. The synchrotron peak frequency has values between 10^{13} and 10^{17}Hz. The SEDs seem to indicate a synchrotron peak in the NIR. Due to the lack of multiwavelength data here, a detailed description is difficult.

8 DISCUSSION

The three blazars discussed in this paper are highly active, displaying outbursts across the whole EM spectrum. We explored the variability properties of 3C 454.3, 3C 279, and S5 0716+714 using seven telescopes in Bulgaria, India, and Greece during the 2011 through 2014 observing seasons. We also searched for colour variations on IDV and short-term time-scales.

Models to explain diverse time-scale variability are broadly classified as intrinsic and extrinsic. Intrinsic origins of AGN variability are those associated with variations in the accretion flow and the relativistic jet. Extrinsic mechanisms include interstellar scintillations which, due to its frequency dependence, are only relevant in low-frequency radio observations and can therefore not be the case of optical INOV. Another external variability cause is gravitational microlensing, which is achromatic and is unlikely to be the sole cause of IDV (Wagner & Witzel 1995). Possible IDV mechanisms in radio-loud AGN are generally believed to be related to conditions in the jet, while in radio-quiet quasars variability is likely due to the intrinsic variability of the accretion disc or related to a weak blazar component (e.g. Stalin et al. 2005). The absence of IDV may be due to a relatively stable relativistic jet with no irregularities in the jet flow.

The optical and multiwavelength flux variations in blazars, particularly in their high state, are often interpreted in terms of relativistic shocks in the Doppler-boosted relativistic jets pointing at or nearly along our LOS (e.g. Marscher & Gear 1985). In an unsteady jet, various instabilities, including turbulence behind shocks, changes in the direction from the LOS or other geometrical effects occurring within the jets may contribute to the variability of the non-thermal emission from blazars (e.g. Camenzind & Krockenberger 1992; Gopal-Krishna & Wiita 1992). However, the observed variability in the low state, when the non-thermal jet emission is less dominant over thermal emissions from the accretion disc, can sometimes be explained by accretion-disc-based models (Urry & Padovani 1995; Wagner & Witzel 1995; including hotspots or instabilities in or above the accretion discs itself, e.g. Chakrabarti & Wiita 1993). As the blazars are AGNs seen nearly face on, any irregularities related to the accretion disc will be visible directly in the low state.

Blazar emission in the post-outburst stage may be plausibly described in the framework of a shock-in-jet model (e.g. Marscher & Gear 1985; Spada et al. 2001; Graff et al. 2008; Joshi & Böttcher 2011). Most of the blazar emission, especially in the active phase, is believed to be due to their jets lying close to the LOS and hence relativistically Doppler boosted. Shocks propagating down these relativistic jets are likely to play important roles in explaining the observed IDV with emissions due to shock regions emitting over multiple wavebands with variability time-scale decreasing as frequency increases. Disc-induced fluctuations when advected into the

jet could be responsible for the changes in the physical parameters of the jet like its velocity, density, or magnetic field (e.g. Wiita 2006). Even slight variations caused in that way are Doppler boosted by a factor of δ^2 to δ^3 (e.g. Blandford & Rees 1978) whereas the observed variability time-scale is compressed by δ^{-1} (e.g. Gopal-Krishna et al. 2003).

The presence of the quasi-power-law continuum is an indication of the synchrotron nature while flux variability was associated with a hardening of the synchrotron spectrum, implying a hardening of the underlying non-thermal electron distribution. The lack of any time delays among the optical bands is well explained by the small difference of the respective observing frequencies, implying small differences in the dynamical time-scales of the radiating electrons, which are likely shorter than the expected light-travel time across the jet, with typical radial dimensions of the order $R \sim 10^{15}$–10^{16} cm. Thus, any microphysical time delays would be washed out by light-travel time effects, even if the observational sampling rate would enable the detection of such delays. The hardening of the underlying electron distribution, leading to the observed BWB trend, may be well explained by a correlation between increasing synchrotron flux and more efficient electron acceleration, leading to an increased population of the highest energy electrons. A plausible physical mechanism to achieve this would be an increased level of hydromagnetic turbulence in the active region of the blazar jet, which would, to first order, lead to a shortening of the characteristic particle acceleration time-scale. Such a scenario has recently been modelled by Diltz & Böttcher (2014) who showed that individual flaring events caused by such parameter variations would lead to the observed BWB trend, along with an anticorrelation between optical and X-ray fluxes, with X-ray variations lagging the optical variability by up to several hours. This could be tested with future, coordinated optical and X-ray monitoring observations of γ-ray blazars, in particular 3C 454.3. Of course optical variability of BL Lacs could be due to more than one mechanism, i.e. a 'mild chromatic' longer term component and a strongly chromatic shorter term component which are due to Doppler factor variations, and intrinsic variations caused by particle acceleration in the Doppler-boosted relativistic jets (e.g. Mastichiadis & Kirk 2002), respectively.

9 CONCLUSIONS

We have performed multiband optical photometry for the blazars 3C 454.3, 3C 279, and S5 0716+714 between 2011 and 2014 to study flux and spectral variability on intraday, short, and long time-scales.

(1) During our ∼37 nights of monitoring for IDV we have found genuine flux variations, using *C*- and *F*-test, on intraday time-scales for ∼21 nights in *B*, *V*, *R*, or *I* with amplitudes of variability up to 31 per cent for 3C 454.3, 9.2 per cent for 3C 279, and 13.5 per cent for S5 0716+714. Each of the blazars seemed to be in an active stage and highly variable during the time span of our studies. The two FSRQs, 3C 454.3 and 3C 279, both were recently in flaring states during the middle of the year 2014.

(2) The STV was relatively weak for each blazar during our whole monitoring period.

(3) Strong intranight colour variations were found in some colour indices for some nights, but no consistent colour variations were found on a yearly basis.

(4) No significant time lags between the optical wavebands were detected, in agreement with expectations due to the small frequency separations of the optical wavebands.

(5) A BWB trend was observed to be dominant in our objects during our observations. Such flattening of the optical spectrum with increasing flux may be interpreted as being dominated by jet synchrotron emission, where increasing flux is related to a hardening of the underlying non-thermal electron spectrum, possibly indicating an enhanced particle-acceleration efficiency.

(6) The NIR–optical spectral properties of each blazar were studied by generating SEDs for each night with sufficient data points in *B*, *V*, *R*, *I*, *J*, and *K* filters.

ACKNOWLEDGEMENTS

We thank the referee for very useful comments which helped us to improve the manuscript. This paper has made use of up-to-date SMARTS optical/NIR LCs that are available at www.astro.yale.edu/smarts/glast/home.php. SMARTS observations of Large Area Telescope-monitored blazars are supported by Yale University and Fermi GI grant NNX 12AP15G, and the SMARTS 1.3-m observing queue received support from NSF grant AST-0707627. The Steward Observatory AGN studies are supported by Fermi Guest Investigator grants NNX08AW56G, NNX09AU10G, and NNX12AO93G. ACG is partially supported by the Chinese Academy of Sciences Visiting Fellowship for Researchers from Developing Countries (grant no. 2014FFJA0004). HG is sponsored by the Chinese Academy of Sciences Visiting Fellowship for Researchers from Developing Countries (grant no. 2014FFJB0005), and supported by the NSFC Research Fund for International Young Scientists (grant no. 11450110398). MFG acknowledges the support from the National Science Foundation of China (grant no. 11473054) and the Science and Technology Commission of Shanghai Municipality (grant no. 14ZR1447100). This research was partially supported by Scientific Research Fund of the Bulgarian Ministry of Education and Sciences under grant DO 02-137 (BIn 13/09) and by Indo-Bulgaria bilateral scientific exchange project INT/Bulgaria/B-5/08 funded by Department of Science and Technology, India. The Skinakas Observatory is a collaborative project of the University of Crete, the Foundation for Research and Technology – Hellas, and the Max–Planck–Institut für Extraterrestrische Physik. The work of MB is supported by the South African Research Chair Initiative by the National Research Foundation and the Department of Science and Technology of South Africa through SARChI Chair grant no. 64789.

REFERENCES

Abdo A. A. et al., 2010, ApJ, 715, 429
Agarwal A., Gupta A. C., 2015, MNRAS, 450, 541
Aller M. F., Aller H. D., Hughes P. A., 1992, ApJ, 399, 16
Aller M. F., Aller H. D., Hughes P. A., 2003, ApJ, 586, 33
Andruchow I., Cellone S. A., Romero G. E., 2005, Bol. Assoc. Argentina Astron., 48, 434
Bailyn C. D., Depoy D., Agostinho R., Mendez R., Espinoza J., Gonzalez D., 1999, BAAS, 31, 1502
Biermann P. et al., 1981, ApJ, 247, L53
Blandford R. D., Rees M. J., 1978, Phys. Scr., 17, 265
Böttcher M., Principe D., 2009, ApJ, 692, 1374
Böttcher M. et al., 2007, ApJ, 670, 968
Böttcher M., Reimer A., Marscher A. P., 2009, ApJ, 703, 1168
Böttcher M., Reimer A., Sweeney K., Prakash A., 2013, ApJ, 768, 54

Burbidge E. M., Rosenberg F. D., 1965, ApJ, 142, 1673
Bychkova V. S., Kardashev N. S., Boldycheva A. V., Gnedin Y. N., Maslennikov K. L., 2006, Astron. Rep., 50, 802
Camenzind M., Krockenberger M., 1992, A&A, 255, 59
Cardelli J. A., Clayton G. C., Mathis J. S., 1989, ApJ, 345, 245
Chakrabarti S. K., Wiita P. J., 1993, ApJ, 411, 602
Chen X., Pohl M., Böttcher M., 2015, MNRAS, 447, 530
Ciprini S., Tosti G., Raiteri C. M., Villata M., Ibrahimov M. A., Nucciarelli G., Lanteri L., 2003, A&A, 400, 487
Clements S. D., Carini M. T., 2001, AJ, 121, 90
Clements S. D., Jenks A., Torres Y., 2003, AJ, 126, 37
de Diego J. A., 2010, AJ, 139, 1269
Diltz C., Böttcher M., 2014, J. High Energy Astrophys., 1, 63
Eachus L. J., Liller W., 1975, ApJ, 200, L61
Edelson R. A., Krolik J. H., 1988, ApJ, 333, 646
Emmanoulopoulos D., McHardy I. M., Uttley P., 2010, MNRAS, 404, 931
Fan J. H., Lin R. G., 2000, ApJ, 537, 101
Finke J. D., Dermer C. D., 2010, ApJ, 714, L303
Fossati G., Maraschi L., Celotti A., Comastri A., Ghisellini G., 1998, MNRAS, 299, 433
Fuhrmann L. et al., 2006, A&A, 445, L1
Gaur H., Gupta A. C., Lachowicz P., Wiita P. J., 2010, ApJ, 718, 279
Gaur H., Gupta A. C., Wiita P. J., 2012, AJ, 143, 23
Ghisellini G. et al., 1997, A&A, 327, 61
Giommi P., Ansari S. G., Micol A., 1995, A&AS, 109, 267
Giommi P. et al., 1999, A&A, 351, 59
Gopal-Krishna, Wiita P. J., 1992, A&A, 259, 109
Gopal-Krishna, Stalin C. S., Sagar R., Wiita P. J., 2003, ApJ, 586, L25
Graff P. B., Georganopoulos M., Perlman E. S., Kazanas D., 2008, ApJ, 689, 68
Gu M.-F., Ai Y. L., 2011, A&A, 528, A95
Gupta A. C., Banerjee D. P. K., Ashok N. M., Joshi U. C., 2004, A&A, 422, 505
Gupta A. C., Fan J. H., Bai J. M., Wagner S. J., 2008a, AJ, 135, 1384
Gupta A. C. et al., 2008b, AJ, 136, 2359
Gupta A. C., Srivastava A. K., Wiita P. J., 2009, ApJ, 690, 216
Hartman R. C. et al., 1996, ApJ, 461, 698
Hartman R. C. et al., 1999, ApJS, 123, 79
Heidt J., Wagner S. J., 1996, A&A, 305, 42
Hufnagel B. R., Bregman J. N., 1992, ApJ, 386, 473
Jorstad S. G. et al., 2013, ApJ, 773, 147
Joshi M., Böttcher M., 2011, ApJ, 727, 21
Jurkevich I., 1971, Ap&SS, 13, 154
Kinman T. D., 1975, in Sherwood V. E., Plaut L., eds, Proc. IAU Symp. 67, Variable Stars and Stellar Evolution, Reidel, Dordrecht, p. 573
Kirk J. G., Rieger F. M., Mastichiadis A., 1998, A&A, 333, 452
Kranich D. et al., 1999, Astropart. Phys., 12, 65
Lainela M. et al., 1999, ApJ, 521, 561
Larionov V. M., Villata M., Raiteri C. M., 2010, A&A, 510, A93
Liu F. K., Xie G. Z., Bai J. M., 1995, A&A, 295, 1
Maraschi L., Ghisellini G., Celotti A., 1992, ApJ, 397, L5
Marscher A. P., Gear W. K., 1985, ApJ, 298, 114
Marscher A. P. et al., 2008, Nature, 452, 966
Mastichiadis A., Kirk J. G., 2002, PASA, 19, 138
Miller H. R., 1981, ApJ, 244, 426
Montagni F., Maselli A., Massaro E., Nesci R., Sclavi S., Maesano M., 2006, A&A, 451, 435
Nesci R., Massaro E., Maesano M., Montagni F., D'Alessio F., Tosti G., Luciani M., 1998, in Koyama K., Kitamoto S., Itoh M., eds, Proc. IAU Symp. 188, The Hot Universe. Kluwer, Dordrecht, p. 442
Netzer H. et al., 1994, ApJ, 430, 191
Nilsson K., Pursimo T., Sillanpää A., Takalo L. O., Lindfors E., 2008, A&A, 487, L29
Pacciani L. et al., 2010, ApJ, 716, L170
Padovani P., Giommi P., 1995, ApJ, 444, 567
Papadakis I. E., Boumis P., Samaritakis V., Papamastorakis J., 2003, A&A, 397, 565
Papadakis I. E., Villata M., Raiteri C. M., 2007, A&A, 470, 857
Peterson B. M., Wanders I., Horne K., Collier S., Alexander T., Kaspi S., Maoz D., 1998, PASP, 110, 660
Quirrenbach A. et al., 1991, ApJ, 372, L71
Raiteri C. M. et al., 1999, in Raiteri C.M., Villata M., Takalo L. O., eds, Proc. OJ-94 Annual Meeting, Blazar Monitoring towards the Third Millennium. Italy, p. 76
Raiteri C. M. et al., 2001, A&A, 377, 396
Raiteri C. M. et al., 2007, A&A, 473, 819
Raiteri C. M. et al., 2008, A&A, 480, 339
Raiteri C. M. et al., 2011, A&A, 534, A87
Raiteri C. M. et al., 2012, A&A, 545, A48
Rani B. et al., 2010a, MNRAS, 404, 1992
Rani B., Gupta A. C., Joshi U. C., Ganesh S., Wiita P. J., 2010b, ApJ, 719, L153
Rector T. A., Perlman E. S., 2003, AJ, 126, 47
Rieke G. H., Lebofsky M. J., 1985, ApJ, 288, 618
Romero G. E., Cellone S. A., Combi J. A., 1999, A&AS, 135, 477
Sambruna R. M., Maraschi L., Urry C. M., 1996, ApJ, 463, 444
Sasada M. et al., 2010, PASJ, 62, 645
Semkov E. et al., 2010, Bulg. Astron. J., 14, 37
Sillanpää A., Haarala S., Valtonen M. J., Sundelius B., Byrd G. G., 1988, ApJ, 325, 628
Simonetti J. H., Cordes J. M., Heeschen D. S., 1985, ApJ, 296, 46
Smith P. S., 1996, in Miller H. R., Webb J. R., Noble J. C., eds, ASP Conf. Ser. Vol. 110, Blazar Continuum Variability. Astron. Soc. Pac., San Francisco, p. 135
Spada M., Ghisellini G., Lazzati D., Celotti A., 2001, MNRAS, 325, 1559
Stalin C. S., Gupta A. C., Gopal-Krishna, Wiita P. J., Sagar R., 2005, MNRAS, 356, 607
Stetson P. B., 1987, PASP, 99, 191
Stetson P. B., 1992, in Worrall D. M., Biemesderfer C., Barnes J., eds, ASP Conf. Ser. Vol. 25, Astronomical Data Analysis Software and Systems I. Astron. Soc. Pac., San Francisco, p. 297
Terrell J., Olsen K. H., 1972, in Evans D. S., Wills D., Wills B. J., eds, Proc. IAU Symp. 44, External Galaxies and Quasi-Stellar Objects. Reidel, Dordrecht, p. 179
Urry C. M., Padovani P., 1995, PASP, 107, 803
Vercellone S. et al., 2008, ApJ, 676, L13
Vercellone S. et al., 2010, Astron. Telegram, 2995, 1
Vercellone S. et al., 2011, ApJ, 736, L38
Villata M., Raiteri C. M., 1999, A&A, 347, 30
Villata M. et al., 2000, A&A, 363, 108
Villata M. et al., 2002, A&A, 390, 407
Villata M. et al., 2006, A&A, 453, 817
Wagner S. J., Witzel A., 1995, ARA&A, 33, 163
Wehrle A. E. et al., 1998, ApJ, 497, 178
Wehrle A. E. et al., 2012, ApJ, 758, 72
White R. J., Peterson B. M., 1994, PASP, 106, 879
Wiita P. J., 2006, in Miller H. R., Marshall K., Webb J. R., Aller M. F., eds, ASP Conf. Ser. Vol. 350, Blazar Variability Workshop II: Entering the GLAST Era. Astron. Soc. Pac., San Francisco, p. 183
Xie G. Z., Zhou S. B., Li K. H., Dai H., Chen L. E., Ma L., 2004, MNRAS, 348, 831
Zhai M., Zheng W. K., Wei J. Y., 2011, A&A, 531, A90

SUPPORTING INFORMATION

The following supplementary material is available for this article online.

Table 1. Observation log of photometric observations for 3C 454.3.
Table 2. Observation log of photometric observations for the FSRQ 3C 279.
Table 3. Observation log of optical observations for the BL Lac S5 0716+714.
Figure 7. LCs of 3C 279 and S5 0716+714 in the first column, their respective SFs in the middle column (where the X-axis is the time

lag, the Y-axis is the SF value, and a.u. stands for arbitrary unit), and DCFs in the last column (where X-axis is the time lag in days and the Y-axis is the DCF value).

Figure 8. Colour–magnitude plots on intraday timescales for 3C 454.3 and S5 0716+714. The *V* magnitudes are given on the X-axis and the various labelled colour indices are plotted against them for each labelled date of observation (http://mnras.oxfordjournals.org/lookup/suppl/doi:10.1093/mnras/stv1208/-/DC1).

This paper has been typeset from a TEX/LATEX file prepared by the author.